ELSEVIER

Journal of Alloys and Compounds 271–273 (1998) 636–640

Journal of ALLOYS AND COMPOUNDS

Thermodynamic assessment of the Fe–U, U–Zr and Fe–U–Zr systems

Masaki Kurata[a,*], Takanari Ogata[a], Kinya Nakamura[a], Toru Ogawa[b]

[a]*Central Research Institute of Electric Power Industry, Iwado-kita 2-11-1, Komae-shi, Tokyo, 201, Japan*
[b]*Japan Atomic Energy Research Institute, Tokai-mura, Ibaraki-ken, 319-11, Japan*

Abstract

In an attempt to understand the phase formation mechanism at the interface of metal fuel and cladding, the isothermal phase diagrams and chemical potential diagrams of the Fe–U–Zr ternary system were calculated using the optimized interaction parameters of three binary subsystems. The Gibbs energies of solution phases and compounds in the Fe–U and U–Zr systems were calculated through an optimization procedure based on both the experimental thermochemical and phase diagram data. The obtained ternary phase diagrams were consistent with the experimental data, when the Gibbs energies of formation of ternary compounds; $Fe_{0.06}U_{0.71}Zr_{0.23}$ and $Fe_{0.3}U_{0.3}Zr_{0.4}$, were assumed to be -3.7~-4.3 and -16~-17.5 kJ per g-atom, respectively. The calculated chemical potential diagrams described satisfactorily the experimental diffusion path for the $U_{0.8}Zr_{O.2}$/Fe couple at 923 K. © 1998 Elsevier Science S.A.

Keywords: Phase diagram; Fe–U; U–Zr; Fe–U–Zr; Chemical potential diagram

1. Introduction

The U–Pu–Zr ternary alloy fuel has been developed for the future commercial fast reactors. Previous study [1] reported that the melting temperature at the interface between U–Pu–Zr fuel and HT-9 cladding can be as low as 933 K, which is near to the hot spot temperature of the ongoing fast reactor design. Since no liquefaction is acceptable during the steady state, it is essential to identify the critical layer that has the lowest liquefaction temperature among the possible interaction layers between fuel and cladding. Ogata et al. found from their out-of-pile diffusion examination carried out at 923 K [2] that the diffusion path of a U–Zr/Fe couple was quite analogous to that of a U–Pu–Zr/stainless-steel [3], and that the basic mechanism of the phase formation, within the interaction layer, can be described using the simpler Fe–U–Zr system. In the present study we attempt to calculate the phase diagram and the chemical potential diagram for the Fe–U–Zr system to give a theoretical basis to the U–Zr/Fe interaction. Before constructing the ternary isotherm, the binary subsystems; Fe–U and U–Zr, have been assessed using the thermochemical and phase diagram data. For the Fe–Zr system the assessment done by Servant et al. [4] has been applied.

2. Thermodynamic basis and modeling

In the previous phase diagram evaluations for the related systems [5–9], the Gibbs energies of mixing of solution phases and the Gibbs energies of formation of compounds were optimized mainly from the phase boundary data, and the resulting calculated phase diagrams agreed with the experimental ones very well. The calculated thermochemical quantities, however, differed from the experimental data. Those differences are due to the fact that the phase boundary is not directly corresponded to the Gibbs energies but determined from their relative relationship. To calculate the thermochemical quantities adequately as well as the phase diagrams, we assess the Fe–U and U–Zr systems using the Parrot module of the Thermocalc code [10], where the Gibbs energy optimization can be performed not only by using the phase diagram data but the other thermochemical quantities, such as activity, Gibbs energy, and heat capacity as well.

The Scientific Group Thermodata Europe (SGTE) phase stability equations [11] are used for the optimization as the thermodynamic functions of the pure components in their stable states. The pure solid elements at 298.15 K in their

*Corresponding author. Tel: +81 33 4802111; fax: +81 33 4802493; e-mail: kurata@criepi.denken.or.jp

0925-8388/98/$19.00
PII: S0925-8388(98)00176-5

stable form (SER) are chosen as the reference state. The Gibbs energies for metastable states are assumed to be +5 kJ per g-atom higher than SER. The interaction parameters of solution phases are modeled using Redlich–Kister polynomial expression [12].

$$^{\circ}G^{ex,\phi}_{mix}(T) = x_i x_j \sum_{\nu=0}^{n} {}^{\nu}L^{\phi}(x_i - x_j)^{\nu} \quad (1)$$

where the interaction parameter, ${}^{\nu}L^{\phi}$, is defined as a linear function of temperature. The x_i and x_j are the mole fraction of each component. The intermediate phases, such as Fe_2U, FeU_6 and δ-UZr_2, are modeled using a two-sublattice model [13] to indicate the nonstoichiometry. The Gibbs energy of formation per formula unit is given by:

$$G^{\phi} - H^{SER} = {}^{ref}G^{\phi} + {}^{id}G^{\phi} + {}^{ex}G^{\phi} \quad (2)$$

where

$${}^{ref}G^{\phi} = y_i' y_j'' {}^{\circ}G^{\phi}_{i:j} + y_j' y_j'' {}^{\circ}G^{\phi}_{j:j} + y_i' y_i'' {}^{\circ}G^{\phi}_{i:i} + y_j' y_j'' {}^{\circ}G^{\phi}_{j:i} \quad (3)$$

$$^{id}G^{\phi} = RT\{p[y_i' \ln(y_i') + y_j' \ln(y_j')] + q[y_i'' \ln(y_i'') + y_j'' \ln(y_j'')]\} \quad (4)$$

$$^{\circ}G^{ex,\phi} = [y_i' y_j' (y_i'' {}^{\circ}L^{\phi}_{i,j:i} + y_j'' {}^{\circ}L^{\phi}_{i,j:j}) + y_i'' y_j'' (y_i' {}^{\circ}L^{\phi}_{i:i,j} + y_j' {}^{\circ}L^{\phi}_{j:i,j})] \quad (5)$$

Here, y_i', y_j', y_i'' and y_j'' are the respective site fractions of the *i*- and *j*-components in the two sublattices designated by ''and''. The $^{\circ}L^{\phi}_{i,i:j}$, $^{\circ}L^{\phi}_{i,j:j}$, $^{\circ}L^{\phi}_{i,i,j}$ and $^{\circ}L^{\phi}_{j:i,j}$ represent the interaction parameters between two components on a given sublattice for a given occupancy by one component in the other sublattice.

3. Optimization

3.1. Binary Fe–U and U–Zr systems

The Fe-U phase diagram was recently summarized by Okamoto [5] taking into account the experimental data [14–18]. Concerning the thermochemical data, the activity in the liquid phase [18] and the enthalpy of Fe_2U formation [19,20] were reported. Unfortunately, large degrees of differences were found among the thermochemical data. Yoshihara and Kanno [19] obtained −20.6 kJ per g-atom for the enthalpy of Fe_2U formation at 298 K, whereas, Akhachinskiy [20] reported −10.8 kJ per g-atom. According to Campbell [21], the values in Ref. [19] are consistent with the systematic variation between the heats of formation and the metallic radius ratio for the AB_2-type Laves compounds. Furthermore, the Gibbs energy of Fe_2U formation at its melting point, 1504 K, reported in Ref. [18] is −18.4 kJ per g-atom and in quite good accordance with the value in Ref. [19], −18.5 kJ per g-atom (with reference to β-U and α-Fe). The value of −5.1 kJ per g-atom in Ref. [20] is largely different from those values. Therefore, we concluded that the thermochemical data reported in Refs. [18,19] are reliable and reasonable, and chose them for the present optimization.

The choice of reasonable initial values is very important to conduct efficiently the iterative optimization calculation. We carried out a preliminary least square calculation based on the phase diagram data to obtain the reasonable initial values of the interaction parameters. Since the liquid phase covers the wide region of the Fe–U system and has a lot of equilibriums at invariant temperature, the Gibbs energy of mixing of liquid phase were firstly calculated using the activity data. In the second step, the Gibbs energy of formation of two compounds were optimized using the invariant temperatures and the Gibbs energy of Fe_2U formation on the condition that the parameters for liquid were fixed. The interaction parameters of the bcc, fcc and tetragonal phases were then determined using the invariant temperatures. The solubility in orthorhombic-U was estimated to be negligible. Since the solid solubilities of two compounds are unknown, the interaction parameters for the sublattice were determined by trial and error to represent the reasonable phase boundaries. Finally, all of the derived parameters were comprehensively optimized again using those values as the initial input.

The calculated Fe–U phase diagram is indicated with the experimental data in Fig. 1(a). The results are in extremely good agreement with the experimental phase boundaries. Fig. 1(b) indicates the variation of the Fe and U activities at 1600 K. The open circles indicate the experimental data points. The solid and dotted lines show the activities calculated in the present study and the other calculations, respectively. The present values agree extremely well with the experimental data where the negative deviation from the Raoult's law are observed. The activities in the other calculations are, on the other hand, slightly larger than the experimental data except for the U activity in the U-rich portion. The Gibbs energies of Fe_2U formation at 998 K (eutectic temperature between Fe_2U and FeU_6) and 1504 K (melting temperature of Fe_2U) are summarized in Table 1. The present calculated values are much closer to the experimental ones at both temperatures, especially to the values in Ref. [19]. The other calculated and estimated values are too positive. Those facts suggest that the thermodynamic quantities calculated in the present study can cover adequately the whole temperature range that appears in the metallic fuel.

For the U–Zr system, the optimization was carried out in the similar manner with the Fe–U system using the phase diagram data [23–26], the activity data in the liquid phase [26] and the heat capacity data [27,28]. The calculated U–Zr phase diagram is compared with the experimental phase boundaries as shown in Fig. 2(a) and the result is satisfactory. Fig. 2(b) indicates the calculated activity at 1823 K with the experimental data points and

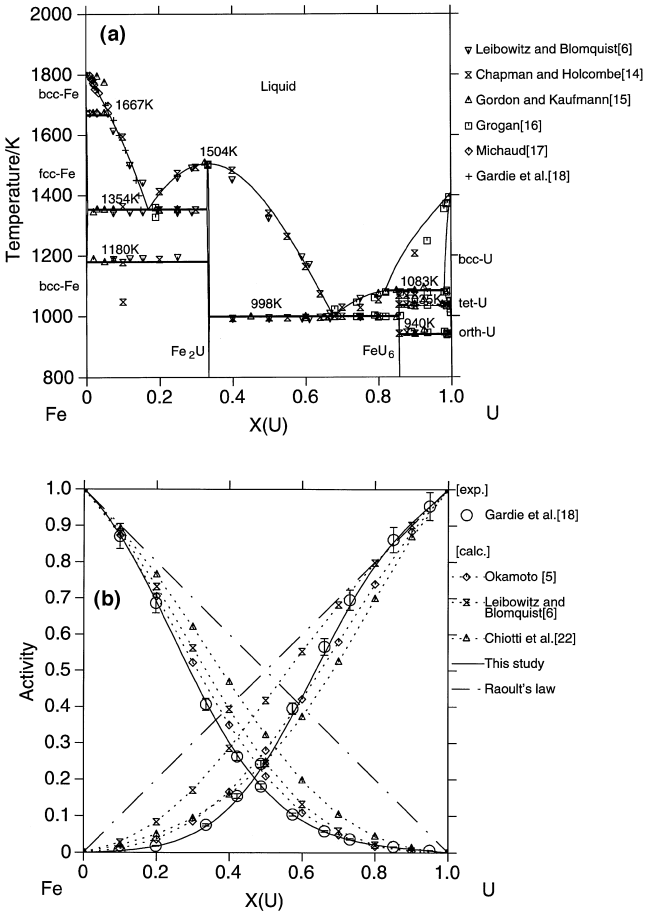

Fig. 1. (a) Calculated Fe–U phase diagram as compared with the experimental data points. (b) Calculated and experimental activity of Fe and U at 1600 K.

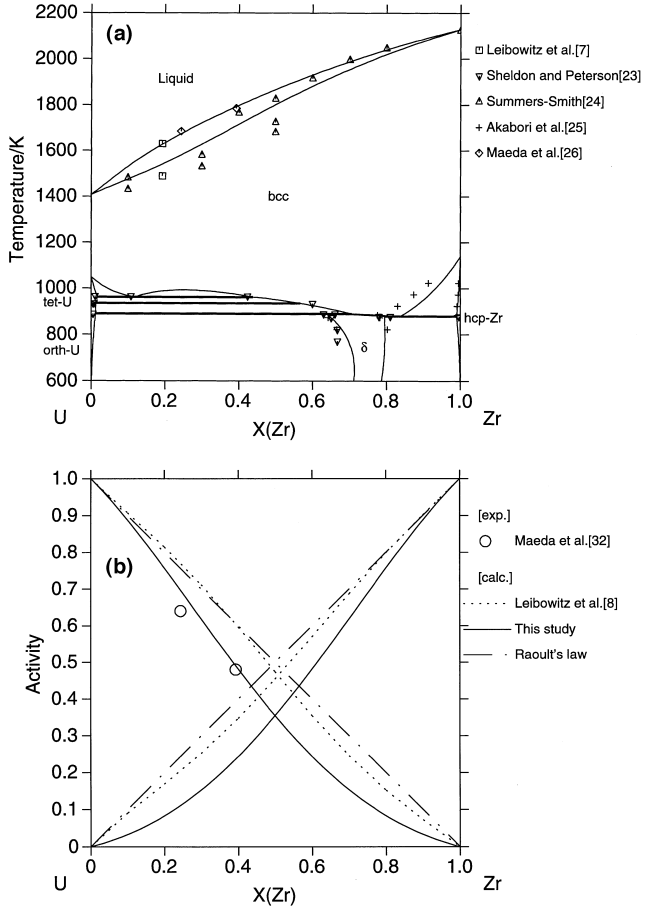

Fig. 2. (a) Calculated U–Zr phase diagram as compared with the experimental data points. (b) Calculated and experimental activity of U and Zr at 1823 K.

the other calculated value. The present calculation reveals the negative deviation from Raoult's law and the derived activity curve for U is close to the experimental values. The other calculation is, on the contrary, closer to Raoult's law but larger than the experimental values.

3.2. Ternary Fe–U–Zr system

The experimental data for the ternary system are quite limited. A partial isotherm at 1073 K has been reported in Ref. [29], where a ternary compound, designated by ε, was found around the center. A recent annealing and quenching study [30] found another ternary compound, designated by λ, near the U-rich corner and indicated the composition of ε and λ to be around $Fe_{0.3}U_{0.3}Zr_{0.4}$ and $Fe_{0.06}U_{0.71}Zr_{0.23}$, respectively. We estimated the Gibbs energies of formation of ε and λ in the following manner. The hypothetical phase boundaries were firstly calculated using the optimized parameters for three binary subsystems, assuming no ternary compound formations and negligible ternary interaction parameters. Then, the Gibbs energies for ε and λ were adjusted to reproduce exactly the experimental tielines.

Table 1
Gibbs energy of Fe_2U formation (with reference state to β-U and α-Fe)

Temperature (K)	Gibbs energy of Fe_2U formation (kJ per g-atom)					
998	−20.1	−17.9	−20.0	−13.0	−14.7	−5.4
1504	−18.8	−18.4	−18.5	−13.4	−15.7	−3.1
Method	Calc.	Exp.	Exp.	Est.	Calc.	Calc.
Reference	This study	[18]	[19]	[22]	[5]	[6]

Fig. 3 indicates the calculated Fe–U–Zr system at 923 K (typical value for the maximum cladding temperature). The thin dotted and solid lines correspond to the hypothetical and modified phase boundaries. The bold dotted lines indicate the experimental diffusion path. Based on the experimental data [29,30], the following tielines were considered to exist in the Fe–U–Zr triangle: from FeU_6 to Fe_2Zr, from FeU_6 to ε, from orthorhombic-U to ε, and from λ to ε. The Gibbs energies of formation of ε and λ, were, therefore, estimated by trial and error to be $-16\sim-17.5$ and $-3.7\sim-4.3$ kJ per g-atom with respect to SER, respectively, when the tielines noted above are maintained.

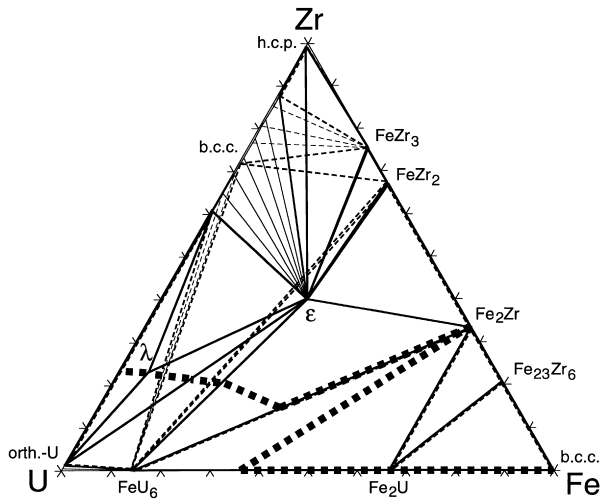

Fig. 3. Calculated Fe–U–Zr ternary isothermal section at 923 K, assuming that ε- and λ-phases exist. Thin dotted lines indicate the hypothetical tielines and the bold dotted lines correspond to the experimental diffusion path quoted from Ref. [2].

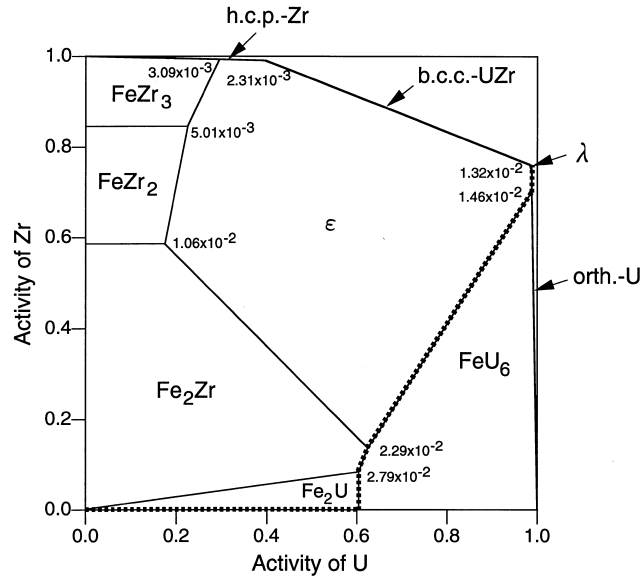

Fig. 4. Chemical potential diagram of the Fe–U–Zr system at 923 K. Dotted line indicates the experimental diffusion path quoted from Ref. [2].

If the Gibbs energy of ε were significantly more negative than the estimated value, the observed tieline, from FeU_6 to Fe_2Zr, should be exchanged to another tieline, from ε to Fe_2U, which is inconsistent with the experimental observation. On the contrary, if it were significantly positive, than the estimated value, ε should disappear from the diagram. These two extremes correspond to the variation in the Gibbs energy of formation of ε within 1.5 kJ per g-atom. A similar situation occurred for λ, and the error is estimated to be within 0.6 kJ per g-atom.

4. Discussion

The chemical potential diagram indicates the activity of each component in the existing phases. To explain thermodynamically the experimental diffusion path shown as a dotted line in Fig. 3(b), we tried to construct a chemical potential diagram for the Fe–U–Zr system. The results are shown in Fig. 4 with the experimental diffusion path. The horizontal and vertical axis are the activity of U and Zr, respectively. A single-phase region is represented by a plane in the ternary chemical potential diagram, because they are treated as stoichiometric compounds. Two-phase and three-phase regions are indicated as lines and points, respectively, due to the phase rule. The values given in the figure correspond to the activity of Fe in each three-phase region.

In the diffusion test, two kinds of layer with negligible amount of Zr were observed in the Fe-rich side and they were identified to be Fe_2U single-phase and Fe_2U/FeU_6 two-phase layers, respectively. Those layers correspond to the line from the origin to the two-phase region of Fe_2U and FeU_6 in Fig. 4. The two-phase layer consisting of Fe_2U and FeU_6 exists even in the U–Zr/Fe diffusion path and the liquefaction temperature is, therefore, estimated to be almost the same as the eutectic point of the Fe–U system (998 K), indicating that the significant decrease in the liquefaction temperature observed in the U–Pu–Zr/HT-9 couple is considered to originate from the contribution of Pu. Further study for the Pu containing system is required to determine the exact liquefaction temperature of metal fuel/cladding interaction.

Some layers were found in the diffusion test next to the Fe_2U/FeU_6 layer, however, the compositions were not clearly identified because very fine grains were dispersed in the layers. They were estimated in the present calculation to be FeU_6/Fe_2Zr, FeU_6, ε/orth.-U, and λ/orth.-U layers. Those layers are drawn as lines in Fig. 4 where the activities of all components vary monotonously.

5. Summary

Taking into account not only the phase diagram data but the thermochemical data, the thermodynamic assessment for the Fe–U and U–Zr binary systems was carried out to obtain an optimized set of interaction parameters. The calculated phase diagrams and thermochemical data were quite satisfactory with regard to the experimental data. A reasonable Fe–U–Zr ternary phase diagram was then drawn using the parameters of binary subsystems and the estimated Gibbs energies of two ternary compounds. The chemical potential diagram described reasonably the experimental diffusion path.

Acknowledgements

The authors gratefully thank Dr. A. Akabori and Mr. A. Itoh, Japan Atomic Energy Research Institute, Mr. T. Yokoo, Central Research Institute of Electric Power Industry, and associate Prof. Dr. M. Hasebe, Kyusyu Institute of Technology, for the offer of valuable experimental data and for the helpful discussion. Grateful acknowledgment must be made to Dr. C. Servant for his permission to use the optimized parameter for the Fe–Zr system.

References

[1] A.B. Cohen, H. Tsai, L.A. Neimark, J. Nucl. Mater. 204 (1993) 244–251.
[2] T. Ogata, K. Nakamura, M. Kurata, A. Itoh, A. Akabori, K. Yokoo, J. Nucl. Mater (to be published).
[3] D.D. Keiser, M.C. Petri, Proc. l5th Annual Conf. Canadian Nucl. Soc., Vol. 2, 1994.
[4] C. Servant, C. Gueneau, I. Ansara, J. Alloys Comp. 220 (1995) 19–26.
[5] H. Okamoto, in: M.E. Kassner D.E. Peterson (Eds.), Phase Diagrams of Binary Actinide Alloys, The Materials Information Society, Materials Park, OH 44073, 1995, pp. 164–168 and 246–247.
[6] L. Leibowitz, R.A. Blomquist, J. Nucl. Mater 184 (1991) 47–52.
[7] L. Leibowitz, R.A. Blomquist, A.D. Pelton, J. Nucl. Mater 167 (1989) 76–81.
[8] A.D. Pelton, L. Leibowitz, R.A. Blomquist, J. Nucl. Mater 201 (1993) 218–224.
[9] T. Ogawa, T. Iwai, J. Less-Common Metals 170 (1991) 101–108.
[10] B. Jansson, PhD Thesis, Royal Institute of Technology, Stockholm, 1984.
[11] A.T. Dinsdale, Calphad 15(4) (1991) 317–425.
[12] O. Redlich, A. Kister, Ind. Eng. Chem. 40 (1948) 345.
[13] B. Sundman, B. Jansson, J.-O. Andersson, Calphad 2(9) (1985) 153.
[14] L.R. Chapman, C.E. Holcombe Jr., J. Nucl. Mater. 126 (1984) 323–326.
[15] P. Gordon, A.R. Kaufmann, Trans. AIME 188 (1950) 182–194.
[16] J.D. Grogan, J. Inst. Met. 77 (1950) 571–576.
[17] G.G. Michaud, Can. Metall. Q 5 (1966) 355–365.
[18] P. Gardie, G. Bordier, J.J. Poupeau, L. Le Ny, J. Nucl. Mater. 189 (1992) 97–102.
[19] K. Yoshihara, M. Kanno, J. Inorg. Nucl. Chem. 36 (1974) 309–312.
[20] V.V. Akhachinskiy, L.M. Kopytin, M.I. Ivanov, N.S. Poldol'skaya, Symposium on the Thermodynamics of Nuclear Materials, IAEA, Vienna, 1962, p. 309.
[21] G.M. Champbell, Metall. Trans. A 8 (1977) 1493.
[22] P. Chiotti, V.V. Akhachinskiy, I. Ansara, M.H. Rans, The Chemical Thermodynamics of Actinide Elernents and Compounds, Part 5 — The Actinide Binary Alloys, IAEA, Vienna, 1981.
[23] R.I. Sheldon, D.E. Peterson, Bull. Alloy Phase Diagrams 10 (1989) 15–171.
[24] D. Summers-Smith, J. Inst. Met. 83 (1954) 277–282.
[25] A. Akabori, A. Itoh, T. Ogawa, F. Kobayashi, Y. Suzuki, J. Nucl. Mater 188 (1992) 249–254.
[26] A. Maeda, Y. Suzuki, T. Ohmichi, J. Alloys Comp. 179 (1992) L25–L27.
[27] Y. Takahashi, K. Yamamoto, T. Ohsato, H. Shimada, T. Terai, M. Yamawaki, J. Nucl. Mater. 167 (1989) 147–151.
[28] T. Matsui, T. Natsume, K. Naito, J. Nucl. Mater. 167 (1989) 152–159.
[29] C.M. Walter, L.R. Kelman, S.T. Zegler, ANL Annual Progress Report for 1965 Metallurgy Division, ANL-7155, 1965, pp. 22–24.
[30] K. Nakamura, M. Akabori, A. Itoh, unpublished work.